

# A Glu209Lys substitution in DRG1/TaACT7, which disturbs F-actin organization, reduces plant height and grain length in bread wheat

Zhencheng Xie\* , Lichao Zhang\* , Qiang Zhang , Yan Lu, Chunhao Dong , Danping Li , Xu Liu, Chuan Xia  and Xiuying Kong 

State Key Laboratory of Crop Gene Resources and Breeding, Institute of Crop Sciences, Chinese Academy of Agricultural Sciences, Beijing, 100081, China

## Summary

Authors for correspondence:

Xu Liu

Email: [liuxu03@caas.cn](mailto:liuxu03@caas.cn)

Chuan Xia

Email: [xiachuan@caas.cn](mailto:xiachuan@caas.cn)

Xiuying Kong

Email: [kongxiuying@caas.cn](mailto:kongxiuying@caas.cn)

Received: 13 March 2023

Accepted: 14 August 2023

New Phytologist (2023)

doi: 10.1111/nph.19246

**Key words:** actin, grain shape, map-based cloning, plant height, wheat.

- Plant height and grain size are two important agronomic traits that are closely related to crop yield. Numerous dwarf and grain-shape mutants have been studied to identify genes that can be used to increase crop yield and improve breeding programs.
- In this study, we characterized a dominant mutant, *dwarf and round grain 1* (*drg1-D*), in bread wheat (*Triticum aestivum* L.). *drg1-D* plants exhibit multiple phenotypic changes, including dwarfism, round grains, and insensitivity to brassinosteroids (BR). Cell structure observation in *drg1-D* mutant plants showed that the reduced organ size is due to irregular cell shape.
- Using map-based cloning and verification in transgenic plants, we found that a Glu209Lys substitution in the DRG1 protein is responsible for the irregular cell size and arrangement in the *drg1-D* mutant. DRG1/TaACT7 encodes an actin family protein that is essential for polymerization stability and microfilament (MF) formation. In addition, the BR response and vesicular transport were altered by the abnormal actin cytoskeleton in *drg1-D* mutant plants.
- Our study demonstrates that DRG1/TaACT7 plays an important role in wheat cell shape determination by modulating actin organization and intracellular material transport, which could in the longer term provide tools to better understand the polymerization of actin and its assembly into filaments and arrays.

## Introduction

Wheat yield is an important component of global food security, which has profound social and economic importance. Considerable effort has been directed toward improving agronomic traits to increase wheat yield. The introduction of semidwarfing genes into wheat was a major success in breeding cultivars with higher yield during the 'Green Revolution' (Hedden, 2003). Grain shape is also an important agronomic trait in wheat, and it influences grain yield and quality in cereal crops (Wang *et al.*, 2018; Li *et al.*, 2019).

As more genes related to these two agronomic traits are being identified and characterized, some genes have been found to affect both plant height and grain size. These genes can influence cell shape and organ size throughout the plant, and many of them are related to hormone signaling. For example, the rice mutants *d2*, *d11*, and *brd1* all display dwarf stature, short grains, and other BR-deficient phenotypes. The causal genes *D2*, *D11*, and *BRD1* all function in BR biosynthesis (Mori *et al.*, 2002; Hong

*et al.*, 2003; Tanabe *et al.*, 2005). Overexpression of GSK3, the ortholog of the BR signaling key factor BIN2, reduced plant height and grain length in rice (Tong *et al.*, 2012). The *Small Grain 2* encodes a ribonuclease H-like domain, which is a positive regulator downstream of GSK2 in response to BR signaling, and its mutation causes insensitivity to exogenous BR treatment (Huang *et al.*, 2022). A protein of unknown function in rice, SHORT GRAIN1, can also decrease organ size and is probably involved in BR signaling (Nakagawa *et al.*, 2012). *Pow1* leads to increased rice grain size via POW1-TAF2 and leaf angle via POW1-BR (Zhang *et al.*, 2021). The E3 ligase activity-related protein DWARF AND SHORT GRAIN 1 (DSG1) in rice might not only participate in the BR pathway but may also be involved in some other hormone pathways (Wang *et al.*, 2017). In wheat, few genes affecting both plant height and grain size have been cloned. TaSG-D1 is an ortholog of BIN2 in wheat, and a gain-of-function mutation in *TaSG-D1* caused the dwarf and round grain phenotype in *Triticum Sphaerococcum* (Cheng *et al.*, 2020). ZnF is a positive regulator for BR signaling, and the edited *znf-bb* mutant in wheat presents reduced plant height and short grain (Song *et al.*, 2023). Defects in the auxin response

\*These authors contributed equally to this work.

transcription factor SMOS1 have been shown to decrease cell size and disrupt normal microtubule orientation (Aya *et al.*, 2014). VILLIN2 (VLN2) is also required for normal cytoskeleton formation and polar auxin transport. A defect in VLN2 resulted in abnormal cell shape and twisted organs (Wu *et al.*, 2015). Studies of SMOS1 and VLN2 have shown that the cytoskeleton is an important regulator of cell shape and organ size in plants.

Actin is a cytoskeletal protein that is conserved in all eukaryotes (Meagher *et al.*, 1999). Actin plays essential roles in several biological processes in plants, including cellular signaling, cell adhesion, mitotic and meiotic cell division, cell expansion, organelle movement, vesicle trafficking, and the establishment of polar cell growth (Pollard & Cooper, 2009). Mutations in actin and associated proteins often result in abnormal cell shape and twisted organogenesis (Li *et al.*, 2003, 2014; Nishimura *et al.*, 2003; Buschmann *et al.*, 2004; Kato *et al.*, 2010; Cvrčková *et al.*, 2015; Feng *et al.*, 2015; Zhu *et al.*, 2016; Sun *et al.*, 2017, 2019; Thyssen *et al.*, 2017; Cao *et al.*, 2021). A T-DNA insertion in *AtACT2* was shown to influence filamentous actin (F-actin) polymerization and root development in *Arabidopsis* (Nishimura *et al.*, 2003). In the *fiz1* mutant, a Glu272Lys substitution in *AtACT8* also has a significant negative effect on actin polymerization. This mutation results in actin filaments with many curled side branches, which disturbs organelle transport (Kato *et al.*, 2010). A single mutation that causes a Gly65Val substitution in the actin gene *GhACT\_L11* in cotton led to dwarf plants with crinkled leaves due to the abnormal organization of F-actin (Thyssen *et al.*, 2017; Sun *et al.*, 2019; Cao *et al.*, 2021). A mutation in the *Rice Morphology Determinant (RMD)* gene altered the configuration of the F-actin array direction and the localization of OsPIN (Li *et al.*, 2014). TWISTED DWARF1 (TWD1) determines the downstream locations of auxin efflux transporters by adjusting actin filaments (Zhu *et al.*, 2016). Many studies have focused on the function of actin and related proteins in cell development, but our understanding of actin is still hindered by the redundancy of actin genes and lethal mutations in actin proteins. The cellular basis of microfilament (MF) function in organogenesis, and the effect of changes in globular actin (G-actin) structure on MF structure, remains largely unclear, especially in crop plants.

Here, we report the isolation and characterization of a dominant wheat mutant, *drg1-D*. *drg1-D* plants display dwarfism, round grains, and BR-insensitive phenotypes that are controlled by a semidominant gene. A G-to-A mutation was identified at position 625 in the *DRG1* coding sequence using map-based cloning. This mutation is predicted to cause a Glu209Lys substitution in the DRG1 protein. Transgenic wheat plants expressing the genomic *drg1-D* gene (*gdrg1-D*) carrying the mutation, and plants in which *DRG1* had been mutated by gene editing confirmed that the DRG1<sup>E209K</sup> amino acid substitution, affected actin organization and caused the abnormal phenotypes observed in *drg1-D* mutant plants, which give us a deeper understanding of the mechanisms controlling proper actin structures required for efficient cell and organ growth. Further analysis showed that BR responses and vesicular transport are interrupted in the *drg1-D* mutant. These findings demonstrate that the DRG1<sup>E209K</sup>

protein reduced plant height in varying degrees and generated strong stem strength through regulating cell shape in the stem, which may have the potential to be used in agronomic trait improvement in wheat.

## Materials and Methods

### Plant materials

The dwarf and round grain mutant *drg1-D* was identified from a large plant population in an EMS-mutagenized wheat mutant library in the background of a common wheat (*Triticum aestivum* L.) cultivar ‘YanZhan1’ (YZ1). Two F<sub>2</sub> mapping populations were produced from crosses between the *drg1-D* mutant and the two wheat cultivars 10th12 and NX188. The F<sub>2</sub> and F<sub>3</sub> mapping populations and T<sub>0</sub>–T<sub>3</sub> generation transgenic plants were planted in the experimental field of the Chinese Academy of Agricultural Sciences, located in Beijing.

### Cellular analysis

The peduncle of YZ1 and *drg1-D* plants was collected after the wheat heading stage. The stems were fixed in 70% FAA, after which the samples were dried in a critical-point drier (Hitachi HCP-2), dissected under a microscope (Leica S8APO; Leica Microsystems, Wetzlar, Germany), and sputter-coated with platinum. The structural features of the stem sections were observed using a scanning electron microscope (SEM; Hitachi S-3000 N; Hitachi High-Technologies Corp., Tokyo, Japan). IMAGEJ software was used to measure cell length and width.

### Phenotypic analysis

The length, width, and thickness of grain and diameter and thickness of stem were measured with a Vernier caliper. Flag leaf angle was measured using a protractor between the stem under the spike and the flag leaf midrib. Plant height was measured before harvesting, and 10 main spikes were bagged at the same time to measure fertile grain number per spike and grain weight per 1000 grains. Spike number per plant was calculated as the average value of 10 plants.

### Stem strength measurement

At milk stage, 10 uniform stems were selected for each treatment, with their different internodes cut. Then, the YYD-1 strength tester (Zhejiang Top Instrument Co. Ltd, Hangzhou, Zhejiang, China) was used to measure the breaking strength of stems according to previous studies (Peng *et al.*, 2014).

### Map-based cloning of *DRG1*

The public SSR markers for genetic mapping were obtained from the GrainGenes 2.0 website (<https://graingenes.org/GG3/>). Polymorphic SSR markers between the parental lines and the mixed pools with extreme phenotypes were used for screening the

10th12 × *drg1-D* F<sub>2:3</sub> populations. Using the sequences of two markers, wmc432 and wmc336 that showed linkage to the target gene *drg1-D*, we developed 430 new SSR markers based on the *Aegilops tauschii* draft genome sequence (Jia *et al.*, 2013). Seven novel markers were located on the genetic map. For fine mapping, we generated another large NX188 × *drg1-D* F<sub>2</sub> segregating population and developed 443 SSR markers in the region between the wmc432 and msp304 based on IWGSC REFSEQ v.1.0. The SSR marker primers were designed using the website <http://probes.pw.usda.gov/batchprimer3/>. DNA sequencing was used to determine which gene in the 275-kb region carried the mutation and would be a candidate for the *DRG1* gene. Specific primer pairs were designed to amplify the genomic sequences of *DRG1*. The PCR assays were performed with high-fidelity KOD neo polymerase (Toyobo, Japan) for 35 cycles (98°C for 5 min, followed by 35 cycles of 98°C for 10 s, 62°C for 45 s, and 72°C for 30 s, with a single cycle of 72°C for 10 min). The purified PCR products were cloned into the pEASY-Blunt zero vector (Transgene, Beijing, China) and sequenced. DNAMAN and DNASTAR software were used to analyze the nucleotide and amino acid sequences. All mapping primers used in this study are given in Table S1.

### Vector construction

The constructs *pDRG1::gdrg1-D* and *pDRG1::GUS* were generated using the In-Fusion HD cloning system (Clontech, Franklin Lake, NJ, USA) with the corresponding primers (Table S1). For genetic complementation, the *drg1-D* genomic fragment that included a 3414-bp promoter region, 1562-bp coding region, and an 883-bp terminator region was inserted into pCAMBIA3301 using a two-step recombination procedure (step 1, primers Infu-1F/Infu1R; step 2, primers Infu-2F/Infu2R), resulting in *pDRG1::gdrg1-D*. For promoter activity analysis, the 3414-bp promoter region was amplified using the Infu-3F/Infu3R primer pair and cloned into pCAMBIA1305, resulting in *pDRG1::GUS*. To generate the vector for gene editing via CRISPR/Cas9, two sgRNAs were designed in the exon of *DRG1*. The target sites were incorporated into forward and reverse primers, respectively, and the PCR fragment amplified from the intermediate vector pCBC-MT1T2 was inserted into the binary vector pBUE413 using the ‘Golden Gate’ method (Engler *et al.*, 2008; Xing *et al.*, 2014). The plasmid was transformed into the wheat cultivar Fielder.

### Plant transformation

The sequencing-confirmed vectors were transformed into 15-d-old immature embryos of the wheat cultivar ‘Fielder’. The transgenic plants were generated with an *Agrobacterium tumefaciens*-mediated transformation method using licensed protocols of ‘PureWheat’ from Japan Tobacco Inc. (Iwata, Shizuoka, Japan) (Ishida *et al.*, 2015). Nine *pDRG1::gdrg1-D*-positive transgenic plants were obtained in T<sub>0</sub> generation. Three *DRG1* gene editing transgenic plants were obtained in T<sub>0</sub> generation. The statistical analysis of T<sub>0</sub> and T<sub>1</sub> transgenic plants was performed at the grain-filling stage.

### GUS analysis

To analyze the activity of the *DRG1* gene promoter, different tissues of homozygous transgenic T<sub>3</sub>-generation wheat plants were stained in a GUS staining solution (100 mM phosphate buffer pH 7.0, 10 mM EDTA, 1 mM potassium ferricyanide, 0.1% Triton X-100, and 2 mM X-Gluc) overnight at 37°C. The staining reaction was stopped by washing the samples in 70% ethanol, after which they were fixed in FAA (5% formaldehyde, 5% acetic acid, and 80% ethanol) until they were examined under a light microscope.

### RNA extraction and RT-qPCR analysis

Total RNA was extracted from young tissues of YZ1 and *drg1-D* plants using a Direct-zol RNA MiniPrep Kit (Zymo Research, Irvine, CA, USA) according to the manufacturer’s instructions. The quality of the extracted RNA was estimated using a Nano-drop 2000 spectrophotometer (Thermo Scientific, Waltham, MA, USA). Reverse transcription (RT) was performed using 5X-All-In-One RT MasterMix (Abm, Richmond, BC, Canada). RT-qPCR analysis was performed on the Roche Real-Time PCR System (Roche, Mannheim, BW, Germany) using SYBR Premix Ex Taq II (TaKaRa, Kusatsu, Shiga, Japan). *TaGAPDH* was used as the internal control for normalization of gene expression. Relative gene expression was calculated by the 2<sup>-ΔΔC<sub>t</sub></sup> method (Livak & Schmittgen, 2001). The specific primers for used for quantitative RT-PCR are described in Table S1. Each experiment was performed with three biological replicates.

### Phylogenetic analysis

All Arabidopsis actin protein sequences (AtACTIN1–AtACTIN11) were downloaded from the TAIR database. The sequences of homologous proteins to *DRG1* from various species were identified by a BLASTP search of the National Center for Biotechnology Information (NCBI) database. The amino acid sequences were aligned with CLUSTALW (<http://clustalw.ddbj.nig.ac.jp/>), and a phylogenetic tree was constructed using the neighbor-joining method as implemented in MEGAX software with the default parameters. The evolutionary distances were calculated using the Poisson model.

### Molecular modeling of G-actin and F-actin

The molecular model of G-actin was constructed using SWISS-MODEL software (<https://www.swissmodel.expasy.org/>). A previously reported G-actin structure, 3chw.1.A, was used as the template. The polymer structure 6anu.1.E was used as the template to construct an F-actin model, and the SWISS-PDB VIEWER software was used to simulate the structural changes caused by the E209K substitution.

### Luciferase complementation imaging (LCI) assay

An LCI assay was performed with the pCAMBIA-nLUC and pCAMBIA-cLUC vectors (Chen *et al.*, 2008) to detect the

DRG1 and DRG1<sup>E209K</sup> interactions in leaf cells of *Nicotiana benthamiana*. The firefly luciferase (LUC) enzyme was divided into the N-terminal part (nLUC) and C-terminal part (cLUC). The full-length coding sequences of *DRG1* and *gdr1-D* (genomic copy carrying the G-to-A mutation) were cloned into the vectors pCAMBIA1300-nLUC and pCAMBIA1300-cLUC, respectively. The nLUC and cLUC tags were fused to the C terminus and N terminus of the full-length DRG1 and *gdr1-D* proteins, respectively. The primers used in this experiment are given in Table S1. Cell suspensions of *Agrobacterium tumefaciens* strain GV3101 carrying the various constructs were co-infiltrated into *N. benthamiana* leaves. A low-light-cooled CCD imaging apparatus (Night SHADE LB 985; Berthold, Bad Wildbad, Germany) with INDIGO software was used to capture the LUC images. At least six independent leaves were used for each experiment, and three biological replications were performed, all with similar results.

### Protein extraction and immunoblotting

Total proteins were extracted in an extraction buffer consisting of 125 mM Tris-HCl (pH 6.8), 4% SDS, 20% glycerol, and 0.001% bromophenol blue.  $\beta$ -mercaptoethanol was added (2% v/v) immediately before use. Anti-MAbGPa (1 : 2000; Sigma, St. Louis, MO, USA) and Anti-MAb2345a (1 : 2000; Sigma) antibodies and an anti-mouse IgG antibody (1 : 75 000; A9044-2ML; Sigma) were used for the detection of the actin protein. An anti-HSP70 antibody (1 : 5000; CW0264M; Cwbio, Taizhou, Jiangsu, China) was used as a loading control. Three replicates, each consisting of 0.5 g wheat leaf tissue, were used for protein extraction.

### Staining and quantification of MFs

Microfilaments (MFs) can be stained with a special marker, Alexa Fluor-488-Phalloidin (Invitrogen, Carlsbad, CA, USA). We used the glycerol method to stain the MFs (Yang *et al.*, 2011). Briefly, 0.5–1 cm root tip segments collected from wheat seedlings 3 d after germination were incubated in PME buffer (100 mM PIPES, 5 mM MgSO<sub>4</sub>, and 10 mM EGTA, pH 6.8) containing 300 mM m-maleimidobenzoyl-N-hydroxysuccinimide ester, 1.5% glycerol, and 0.1% Triton X-100, with gentle agitation for 30 min, followed by rinsing twice with PME. The samples were then fixed in PME supplemented with 2% paraformaldehyde for 30 min, rinsed twice with PME, and finally incubated in actin-staining buffer (PME, 1.5% glycerol, and 0.1% Triton X-100) containing 0.66 mM Alexa Fluor-488-Phalloidin at 4°C in the dark overnight. Immunostaining of MFs was performed according to previously published methods (Yang *et al.*, 2011). For data collection, optical sections were taken with a Zeiss LSM 700 confocal microscope equipped with a 40 $\times$  objective, and the step size was set at 0.4  $\mu$ m to collect optical sections. Alexa Fluor-488-Phalloidin was excited with the 488-nm line of an argon laser with the emission wavelength set to 550–600 nm. Images were prepared by generating projections of the optical

sections through an individual epidermal cell. The average fluorescence intensity of the MFs was examined using IMAGEJ (Higaki *et al.*, 2010). The skewness of MFs was measured according to previously published methods (Li *et al.*, 2012).

### Actin nucleation assay

Actin nucleation assays were conducted according to the published methods (Michelot *et al.*, 2005). Mg-ATP-actin was prepared by incubation of Ca-ATP-actin with 1-mM EGTA and 0.1-mM MgCl<sub>2</sub> for 2 min on ice. Monomeric rabbit skeletal muscle actin (2  $\mu$ M; 10% pyrene-labeled, BK003; Cytoskeleton, Denver, CO, USA) was incubated with different concentrations of DRG1-6 $\times$ His or DRG1<sup>E209K</sup>-6 $\times$ His for 5 min at 25°C. Pyrene fluorescence was detected by a Varioskan LUX Multi-mode Microplate Reader (Thermo Scientific, Waltham, MA, USA) immediately after the addition of one-tenth volume of 10 $\times$  KMEI buffer (500-mM KCl, 10-mM MgCl<sub>2</sub>, 10-mM EGTA, and 100-mM imidazole-HCl, pH 7.0). The fluorescence signal was detected every 60 s for a total of 38 min.

### Transcriptome analysis

Wheat peduncle bases (2 cm) were sampled from 30 homozygous individuals from the YZ1  $\times$  *gdr1-D* BC<sub>2</sub>F<sub>3</sub> segregating population with extreme phenotypes. Total RNA extraction and assessment of RNA quantity were as described in the previous section 'RNA extraction and RT-qPCR analysis'. The barcoded cDNA libraries were constructed and sequenced by Tcuni Inc., Chengdu, China. Approximately 83.2 Gb of raw nucleotide sequence data was obtained. Data processing and analysis were performed according to the methods described in Yang *et al.* (2021).

### Measurements of BR contents

To measure the levels of BR, samples of *c.* 2 g of leaf tissue were collected from 15-d-old YZ1 and *gdr1-D* seedlings that were grown in a growth chamber at 18–20°C (normal growing temperature) with a 16 h : 8 h, light : dark photoperiod. The BR levels including castasterone (CS), 6-deoxoCS, and brassinolide (BL), were quantified at Wuhan Greensword Creation Technology Co. Ltd., (Wuhan, China) using UHPLC-MS/MS analysis (Ultimate 3000 UHPLC coupled with TSQ Quantiva; Thermo Scientific, Waltham, MA, USA). Three biological replicates were analyzed for this experiment.

### Observation of vesicles in root cells

The distribution of vesicles in root cells was investigated using the methods described by Li *et al.* (2014). Root tip sections 1 cm in length were incubated in FM4-64 staining buffer (5 mM) for 30 min at 25°C and then observed under a LSM780 confocal laser microscope (Zeiss, Jena, Germany). The FM4-64 fluorescence was excited at 515 nm, with emission at 640 nm. The average fluorescence intensity of the MF was examined.

## Accession numbers

Sequencing data of this study can be found at the National Center for Biotechnology Information (<https://www.ncbi.nlm.nih.gov/bioproject/>) with the BioProject ID PRJNA930156. The sequences used for phylogenetic analysis were assigned the following TAIR accession nos. AT2G37620, AT3G18780, AT3G53750, AT5G59370, AT5G09810, AT1G49240, AT3G12110, and AT3G46520. The sequences used for analyzing homologous proteins were assigned the following GenBank accession nos. AHE76165, NP\_196543.1, NP\_001399649.1, BAF83305.1, WP\_176232696.1, NP\_116614.1, XP\_015617195.1, NP\_001001409.2, and BAE40656.1.

## Results

### Characterization of the *drg1-D* mutant

We identified a dominant dwarf wheat mutant with round grain (*drg1-D*) from an ethyl methanesulfonate (EMS)-mutagenized population of the wheat variety ‘Yanzhan1’ (YZ1). *drg1-D* mutant plants display dwarfing, round grain, and reduced stem length, spike length, and leaf length throughout the growth period (Figs 1a–h, S1a–i; Table S2). Plant height in the *drg1-D* mutant ( $29 \pm 0.39$  cm) was decreased by 58.6% compared with plants of the parental line YZ1 ( $70 \pm 1.40$  cm; Figs 1b, S1a). Spike length and the number of grains in the mutant decreased by 40% and 27.3%, respectively, compared with YZ1 (Fig. 1b,c; Table S2). Average length of the mutant grains was also decreased by 45.8% compared with YZ1 grains, grain width was similar to that in YZ1, while the grain thickness was increased by 11%, so the *drg1-D* mutant grains are round in shape (Fig. 1d–g). The *drg1-D* mutant plants have twisted and short stems (Fig. 1c), and the length of each internode was reduced, although there was no change in the number of nodes compared with YZ1 (Fig. 1h). The leaves of *drg1-D* mutant plants were wrinkled at the early stage of leaf development (Fig. S1b). Leaf length was reduced compared with YZ1, but leaf width and thickness increased in the *drg1-D* mutant (Fig. S1b,f–h). In addition, the leaf angle was significantly reduced in *drg1-D* mutant plants (Figs 1b, S1i). These reductions in height and leaf angle were very similar to the phenotypes of BR-deficient mutants. Therefore, we treated YZ1 and *drg1-D* plants with epi-brassinolide (BL) to determine the possible effects on leaf angle in seedlings at the second leaf stage. In the dark, YZ1 and *drg1-D* mutant seedlings were soaked in several concentrations of eBL solution (0, 0.02, 0.2, and  $2 \mu\text{mol l}^{-1}$ ) for 72 h. Significant increases in leaf angle in *drg1-D* mutant plants were only observed in seedlings treated with the high concentration of BR ( $0 \mu\text{mol l}^{-1} \leq \text{YZ1} \leq 0.02 \mu\text{mol l}^{-1}$ ,  $\text{drg1-D} \geq 0.02 \mu\text{mol l}^{-1}$ ; Fig. 1i–k). The leaf unrolling response gave a similar result (Fig. S2a,b; Isidro *et al.*, 2012).

To investigate the dwarf plant phenotype in detail, we carried out histological analyses to examine cell length and cell numbers in YZ1 and mutant plants. Compared with YZ1, cell shape and cell size were irregular in cross sections of the *drg1-D* plant stems (Fig. 1l,m). The longitudinal sections of *drg1-D* stems also

showed irregular cell shape and cell size, and the arrangement of cells was disordered (Fig. 1n,o). These observations indicate that the dwarf plant phenotype of the *drg1-D* mutant results from the observed changes in cell shape, cell size, and cell arrangement in both the latitudinal and longitudinal directions. Also, while the stem diameter of *drg1-D* plants decreased, the stem wall thickness and stem strength increased (Figs S1c, S2c–e). The abnormal cell shapes observed in *drg1-D* mutant plants are much severe than those observed in BR-insensitive mutants.

### Map-based cloning of the *DRG1* gene

Our previous results indicated that the mutation in *drg1-D* was inherited in a semidominant manner. Moreover, the dwarf plant and round grain phenotypes of *drg1-D* mutant plants were significantly correlated and are controlled by a single gene (Lu *et al.*, 2014).

The initial mapping of *DRG1* was performed using a segregating  $F_2$  population derived from the cross of the wheat cultivar 10th12 (CIMMYT)  $\times$  *drg1-D* mutant. Using SSR markers and  $F_2:3$  populations, the mutant gene was mapped to a region of wheat chromosome 1DS between the flanking markers wmc336 and wmc432. Following this, 430 new SSR markers were developed based on the *Aegilops tauschii* draft genome sequence (Jia *et al.*, 2013), and seven of the new markers were found to be linked to the *drg1-D* gene (Table S1). The *drg1-D* gene was located between markers wmc432 and msp304 with genetic distances of 0.4 and 1.7 cM, respectively.

In order to narrow the distance between the marker and target gene, fine mapping was performed using another  $F_2$  segregating population derived from the cross ‘NeiXiang188’ (NX188)  $\times$  *drg1-D* mutant that contained 17 065  $F_2$  progeny plants (Fig. 2a). Based on the number of recombinant plants present in the  $F_2$  population, the *drg1-D* gene was mapped to a 275-kb region on chromosome 1DS flanked by marker msp583 and msp712. This region contains seven high-confidence and two low-confidence genes according to IWGSC REFSEQ v.1.0 ([https://urgi.versailles.inra.fr/jbrowseiwgsc/gmod\\_jbrowse/?data](https://urgi.versailles.inra.fr/jbrowseiwgsc/gmod_jbrowse/?data)) (Fig. 2a; Table S3). After sequencing the nine predicted genes (including their promoter and terminator regions), only one single-nucleotide polymorphism (SNP) was identified between the two parental lines, and it was located in the third exon of *TraesCS1D02G020000*. The G-to-A SNP at position 625 of the coding sequence led to a predicted amino acid substitution from glutamic acid (209E) to lysine (209 K; Fig. 2a).

### Verifying the effects of the mutated *DRG1* gene on growth of wheat plants

In order to confirm that the mutant phenotype is caused by the mutation in *TraesCS1D02G020000*, we conducted a transgenic experiment. A 5859-bp genomic DNA fragment containing the full-length sequence of *TraesCS1D02G020000* (including a 3414-bp promoter region, a 1562-bp coding region, and an 883-bp terminator region) with the G-to-A mutation (*gdrg1-D*) was introduced into the wheat cultivar

'Fielder' using *Agrobacterium*-mediated transformation. In the T<sub>0</sub> generation, nine independent transgenic events displayed semidwarf plants (Fig. S3a). The phenotypes of transgenic plants in T<sub>1</sub>–T<sub>2</sub> generations were segregated in plant height (Fig. S3b). Homozygous transgenic wheat plants carrying the

*drg1-D* construct in T<sub>3</sub> generation showed the same phenotypes as *drg1-D* mutant plants, such as dwarfing, round grain and small spike (Figs 2b–h, S3c–i). These results indicated that the phenotypes of the *drg1-D* mutant plants is caused by the mutation in *DRG1*.

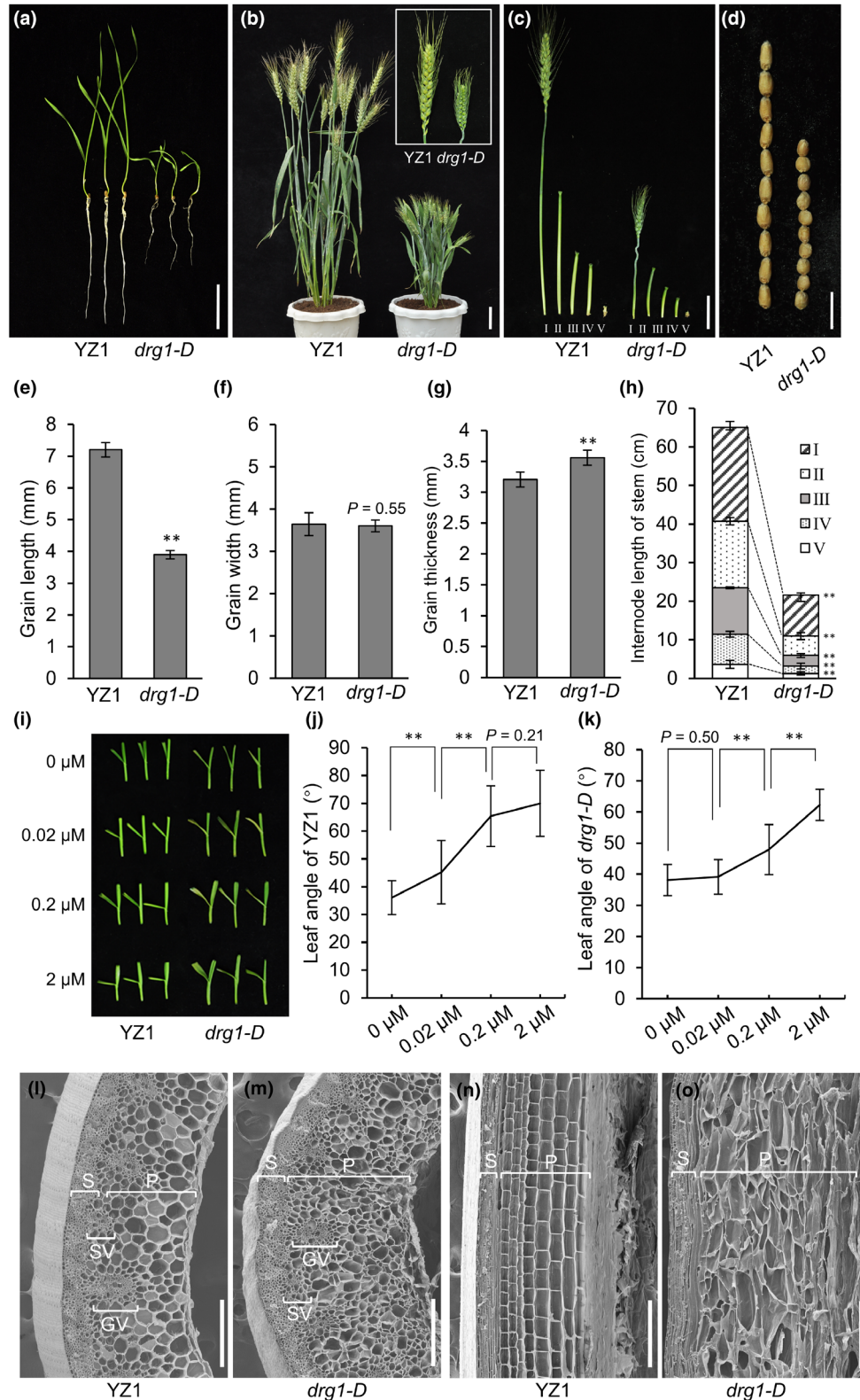


**Fig. 1** Phenotypes of YZ1 and *drg1-D* mutant plants. (a, b) Reduced plant height of *drg1-D* at the seedling and grain-filling stages. Bars: 5 cm. (c) Morphological observation of internodes in YZ1 (left) and the *drg1-D* mutant plants (right). The length of each segment is decreased in the *drg1-D* mutant. Bars: 5 cm. I–V indicate the different internodes. (d) Grain morphology in YZ1 and *drg1-D* plants. The *drg1-D* mutant plants have round grains. Bars: 1 cm. (e–g) Grain length, width, and thickness in the YZ1 and *drg1-D* plants. \*\*,  $P < 0.01$ , significant differences (Student's *t*-test). Error bars indicate SDs ( $n = 20$ ). (h) Internode lengths in the YZ1 and *drg1-D* plants. \*\*,  $P < 0.01$ , significant differences (Student's *t*-test). Error bars indicate SDs ( $n = 10$ ). I–V indicate the different internodes. (i) Leaves of YZ1 and *drg1-D* plants were treated with different concentrations of eBL at the seedling stage for 72 h. The BL concentrations were 0, 0.02, 0.2, and 2  $\mu\text{mol l}^{-1}$ . Three independent biological replicates were used, and each replicate contained 10 seedlings. (j, k) After eBL treatment, the leaf angles were measured. \*\*,  $P < 0.01$ , significant differences (Student's *t*-test). Error bars indicate SDs ( $n = 30$ ). (l–m) Cross sections of YZ1 and *drg1-D* stems showing that the stem cell shapes are irregular and the cell arrangement is disorderly in the *drg1-D* mutant. Bars: 500  $\mu\text{m}$ . (n–o) Longitudinal sections of YZ1 and *drg1-D* stems showing that the stem cell shapes the cell arrangement is disorderly in the *drg1-D* mutant. Bars: 500  $\mu\text{m}$ . GV, great vascular bundle; P, parenchyma; S, sclerenchyma, SV, small vascular bundle.

To further investigate this result, the *DRG1* genes from the three subgenomes were identified (Figs 3a,b, S4). We generated *DRG1*-gene knockout wheat lines using the CRISPR-Cas9 genome editing system. A highly conserved sequence region was edited in all three *DRG1* homologs (all AABDD) in the 'Fielder' genome (Fig. 3c). Three gene-edited lines were identified that had frame-shift mutations in all three subgenomic copies of *DRG1*; these mutations included deletion, insertion, SNP, and sequence inversion (Fig. 3c; Table S4). The edited plants also exhibited decreased plant height and reduced grain length, but the phenotypes were not as severe as those observed in *drg1-D* mutant plants (Figs 3d–i, S5a–g). The results of the gene editing study together with the transgenic *gdrg1-D*-overexpressing plants suggest that the E209K substitution in *DRG1* leads to multiple growth defects in the *drg1-D* mutant.

### Phylogenetic analysis and expression pattern of the *DRG1* gene

The phylogenetic analysis shows that the *DRG1* protein is highly similar to actin family members. *DRG1* has the highest sequence similarity to *AtACT7* (97.35%) indicating *DRG1* is the homologous gene of *AtACT7* (Fig. 4a; Table S5). The eight functional Arabidopsis actin genes can be divided into two classes: vegetative and reproductive. The vegetative class of actin express in nearly all vegetative tissues (McDowell *et al.*, 1996; Meagher *et al.*, 1999). *AtACT7* involved in vegetative organ development and MF organization (McDowell *et al.*, 1996; Meagher *et al.*, 1999).

We performed RT-qPCR analysis to investigate the expression pattern of the *DRG1/TaACT7* gene in different tissues. The *DRG1/TaACT7* gene was found to be expressed in stems, rachides, flag leaves, roots, glumes, lemmas, paleas, stamens, and pistils (Fig. 4b). To further confirm these results, we constructed a fusion plasmid with the promoter region of *DRG1* fused to the GUS reporter gene and introduced the construct into wheat. GUS expression in the transgenic plants was observed in leaves, stems, roots, glumes, lemmas, sheaths, stamens, pistils, and grains and was higher in leaves, stems, and sheaths (Fig. 4c). These results suggest that *DRG1/TaACT7* constitutively expressed in wheat.

### The number of MFs was reduced in the *drg1-D* mutant

To investigate the effect of the mutant protein on MF organization, we selected the root elongation zone for detailed analysis using phalloidin staining. As shown in Fig. 5a,b, numerous

assembled MFs could be stained clearly in the root cells of YZ1 and 'Fielder'. By contrast, the detected MFs were short and thin in root cells of the *drg1-D* mutant and the *pDRG1::gdrg1-D* transgenic line plants (Fig. 5c,d). Measurement of the average fluorescence intensity of MF staining revealed that the number of MFs was significantly decreased in root cells of the *drg1-D* mutant and *drg1-D* gene transgenic lines (Fig. 5e). Skewness of phalloidin staining images was measured to represent the extent of F-actin bundling. The skewness analysis indicated that the F-actin bundling was significantly reduced in *drg1-D* mutant (Fig. 5f). In order to determine whether the reduction in the fluorescent signal of the MFs is caused by the decrease in the amount of *DRG1*, we quantified the expression levels of the *DRG1* and *DRG1*<sup>E209K</sup> monomers. Western blotting results showed that there were no significant differences in total actin levels between wild-type (WT) and the *drg1-D* mutant (Fig. 5g). The expression level of the *DRG1* monomer even increased in the *gdrg1-D* transgenic line, but the number of MFs was lower in the *gdrg1-D* transgenic line (Fig. 5h). Luciferase complementation imaging (LCI) detection of *DRG1* and *DRG1*<sup>E209K</sup> demonstrated that the monomers of the *DRG1*<sup>E209K</sup> protein were able to polymerize in plant cells (Fig. 5i).

To observe actin polymerization *in vitro*, we performed actin nucleation assay. Pyrene-labeled rabbit skeletal actin monomers were incubated with different concentrations of recombinant *DRG1* and *DRG1*<sup>E209K</sup>. The fluorescence, which is directly proportional to the actin filament concentration, was dramatically increased with adding *DRG1* and decreased with adding *DRG1*<sup>E209K</sup> (Fig. 5j). These results indicated that *DRG1*<sup>E209K</sup> disturbs the configuration and bundling of MFs.

### The Glu209Lys substitution in the *DRG1* protein interferes with actin polymerization

To study the *drg1-D* mutation in detail, we performed a protein sequence alignment of *DRG1* and homologous proteins from prokaryotic and eukaryotic species (bacteria, fungi, animals, and plants). The actin proteins from these organisms have > 85% sequence identity with the *DRG1* protein (Fig. 6a). Actin proteins are extremely conserved in all eukaryotic organisms, and Glu209 is highly conserved in all organisms, implying that Glu209 is important to the function of *DRG1* (Fig. 6a).

To gain a deeper understanding of *DRG1*<sup>E209K</sup>, we modeled the tertiary and quaternary structures of *DRG1* monomers and polymers using solved crystal structures of highly homologous

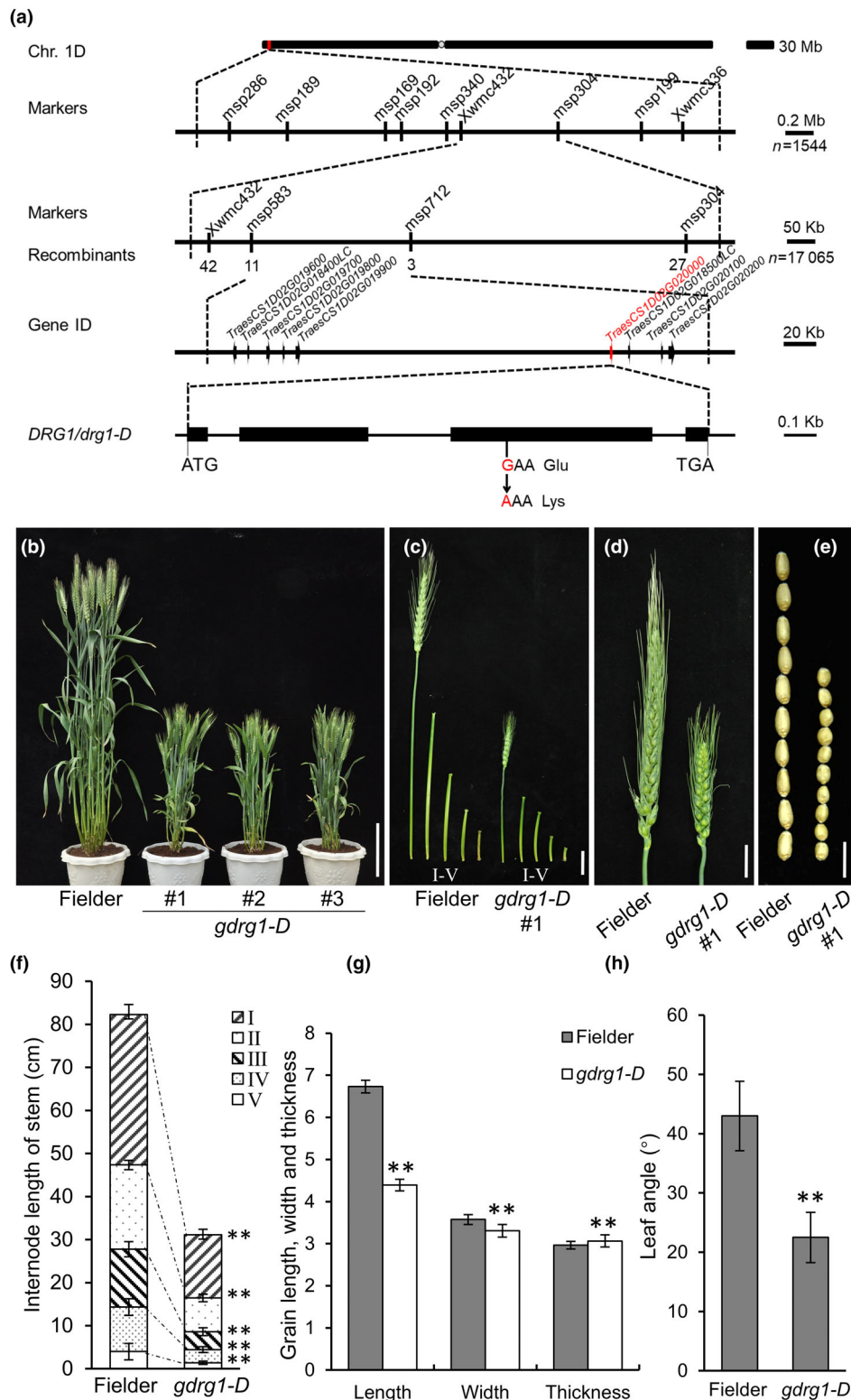


**Fig. 2** Cloning and genetic verification of the *DRG1* gene. (a) Map-based cloning of the *DRG1/drg1-D* gene and gene structure of *DRG1*. The target gene was mapped to the region between the markers *msp583* and *msp712* on chromosome 1DS, and this genomic region was narrowed to c. 275-kb using 17 065  $F_2$  population. There were 11 recombinants and 3 recombinants detected using SSR markers *msp583* and *msp712*, respectively. There were nine predicted genes in this genomic region. *TraesCS1D02G020000* was the only gene with the mutation. The candidate gene *TraesCS1D02G020000* and mutated site are marked with red color. (b–e) Phenotypic characterization of the transgenic plants. Overexpression of the mutant gene *drg1-D* caused a severe phenotype that included dwarfing, short spikes and internodes, and round grains in the transgenic plants. Bars: 5 cm in (b, c), Bars: 1 cm in (d, e). (c, f) Internode lengths in the 'Fielder' and transgenic plants. \*\*,  $P < 0.01$ , significant differences (Student's *t*-test). Error bars indicate SDs ( $n = 10$ ). (g, h) Grain length, width, thickness, and leaf angles in the nontransgenic and the transgenic plants. \*\*,  $P < 0.01$ , significant differences (Student's *t*-test). Error bars indicate SDs ( $n = 30$ ).



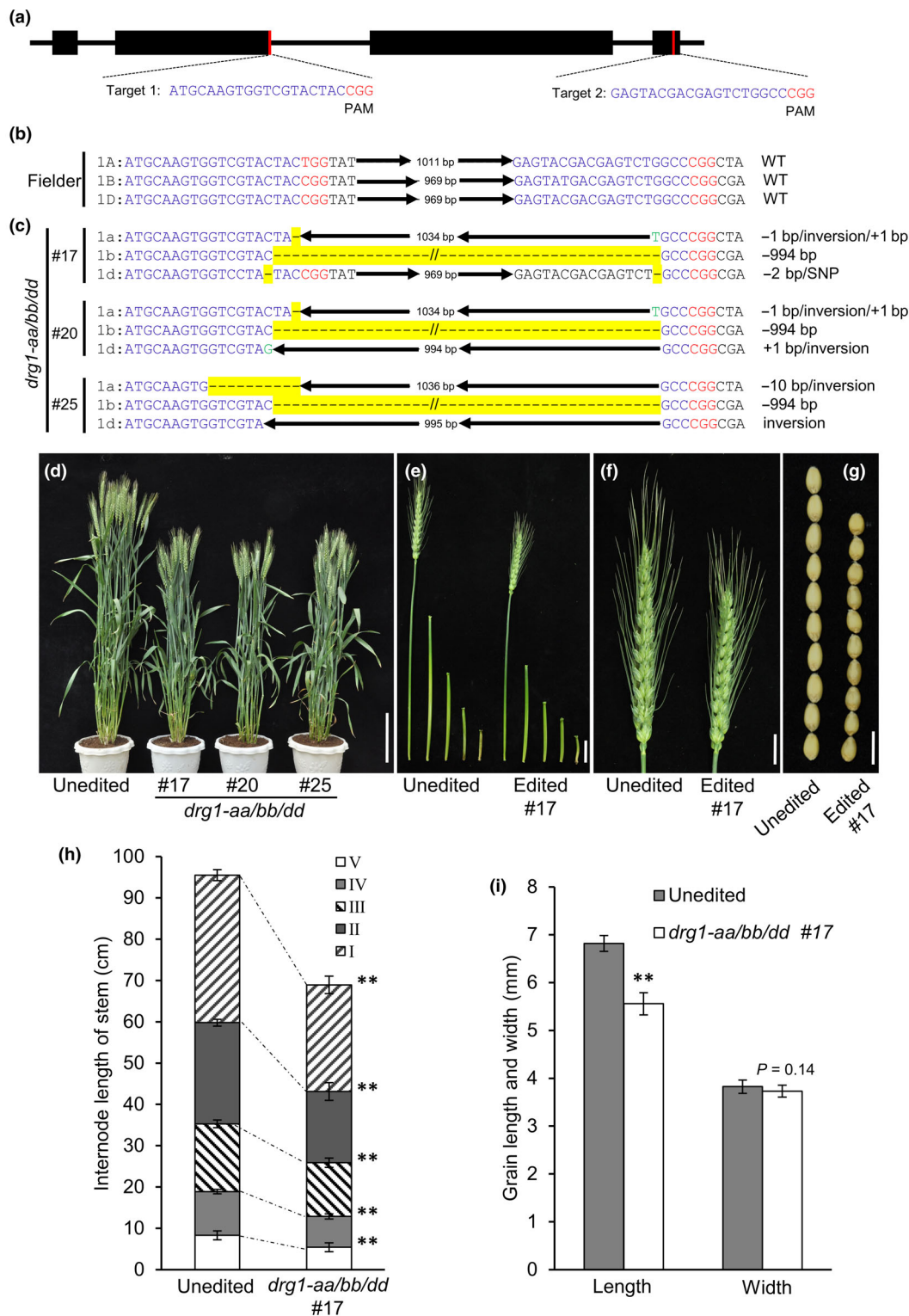


**Fig. 3** Phenotypic analysis of the *DRG1* gene-edited lines. (a) CRISPR/Cas9-induced mutations in the *DRG1*-AA/BB/DD gene loci. The positions and sequences of the target sites for CRISPR/Cas9 gene editing are shown. Red letters indicate the PAM motifs, and blue letters indicate the sgRNA target sequences. (b) Three subgenome reference sequences of *DRG1* gene in 'Fielder'. Black arrows represent the sequence direction. (c) Genotypes of the mutant lines. The symbol '+' and the color green indicate the nucleotide insertions, while the symbol '-' and the color yellow indicate the nucleotide deletions. Inversion indicates that the sequence direction is opposite between the target sites. The base numbers of deletion, insertion, and sequence inversion were shown on the right. SNP, single-nucleotide polymorphism. Black arrows represent the sequence direction. (d–g) Phenotypic observation of the knockout lines and the unedited 'Fielder'. Bars: 10 cm in (d). (e, h) The lengths of every internode are shorter in the gene knockout lines than in unedited 'Fielder'. Bars: 5 cm. \*\*,  $P < 0.01$ , significant differences (Student's *t*-test). Error bars indicate SDs ( $n = 10$ ). (f) Spike lengths of knockout lines were decreased. Bars: 1 cm. (g, i). Grain lengths of knockout lines were decreased, and widths were not changed. Bars: 1 cm. \*\*,  $P < 0.01$ , significant differences (Student's *t*-test). Error bars indicate SDs ( $n = 30$ ).

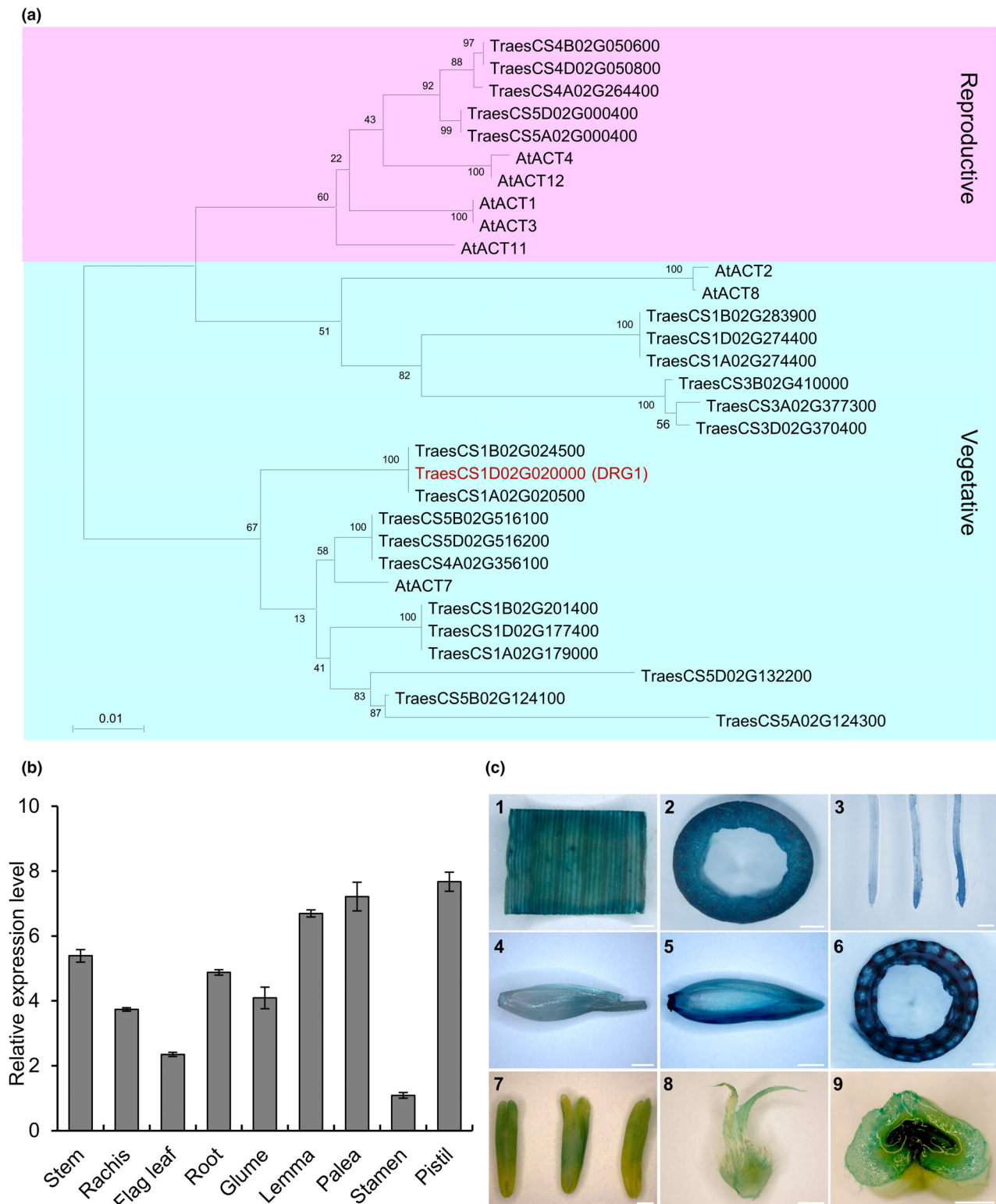


**Fig. 4** Phylogenetic analysis of DRG1-related proteins and expression pattern analysis of *DRG1*. (a) Phylogenetic analysis of proteins similar to DRG1 from *T. aestivum* and ACT family members from *Arabidopsis thaliana*. The phylogenetic tree shows that DRG1 belongs to the vegetative class and is the homolog of AtACT7 from *A. thaliana*. The actin genes belong to vegetative classes strongly expressed in nearly all vegetative tissues, while the genes belong to reproductive classes only expressed in reproductive tissues. The phylogenetic tree was constructed using MEGA X and the neighbor-joining method, and bootstrap values calculated from 1000 replicates are marked on the branch nodes. Branch length represents substitutions per site. The protein ID with red letters indicates the DRG1 protein. (b) RT-qPCR analysis of *DRG1* expression in various wheat tissues. The error bars represent SDs ( $n = 3$ ). (c) GUS activity in vegetative and reproductive tissue of a transgenic wheat line carrying the *pDRG1::GUS* construct. 1–9: leaf, stem, young root, glumes, lemma, sheath, stamen, pistil, and grain. Bars in 6 and 7 = 0.5 mm. Bars in 2, 8 and 9 = 1 mm. Bars in 1, 3, 4, and 5 = 2 mm.

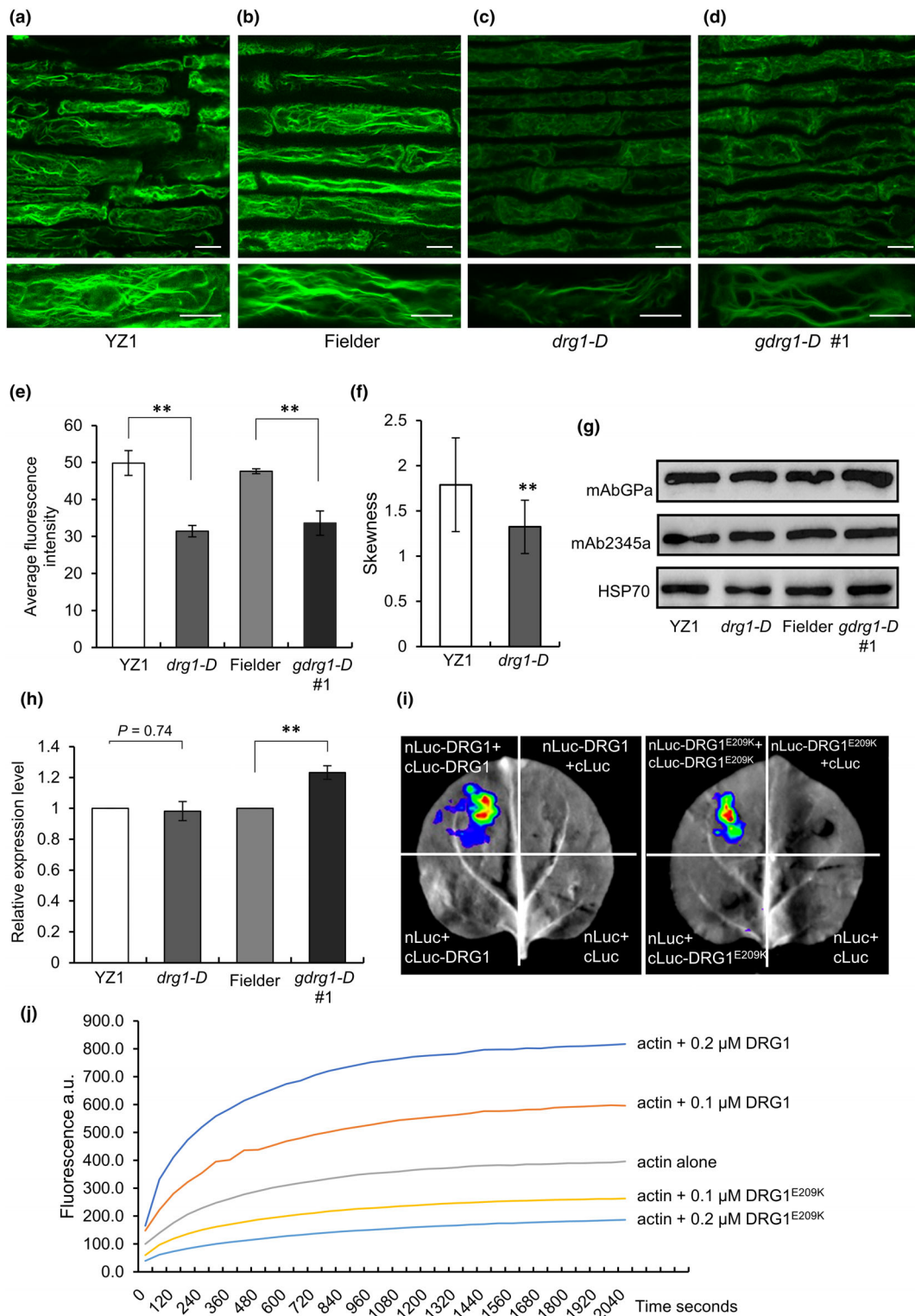


**Fig. 5** Microfilament (MF) observation and DRG1 protein expression analysis. (a–d) Staining of MFs in the root elongation zone by Alexa Fluor-488-Phalloidin in wheat cultivars YZ1 (a), and 'Fielder' (b), the *drg1-D* mutant (c), and the *pDRG1::gdr1-D* transgenic line (d). The maximum projections of all optical sections are shown (0.4-mm intervals). Bars: 10  $\mu$ m. (e) Average fluorescence intensity of MFs analyzed using MBF-IMAGEJ software. \*\*,  $P < 0.01$ , significant differences (Student's *t*-test). Error bars indicate SDs ( $n = 10$ ). (f) Skewness was measured to determine the bundling status of MFs in the YZ1 and *drg1-D*. \*\*,  $P < 0.01$ , significant differences (Student's *t*-test) (g) Protein gel blot analysis of the levels of actin isoforms in leaf samples 10 d after germination. Total actin (first rows) was detected with anti-mAbGPa. DRG1 (second rows) was detected with anti-mAb2345a, which only binds to ACT7. Blots shown in the last rows were probed with an anti-HSP70 polyclonal antibody to show equal protein loading. (h) Relative expression level of DRG1 in YZ1, *drg1-D* mutant, 'Fielder', and the transgenic plants. \*\*,  $P < 0.01$ , significant differences (Student's *t*-test). Error bars indicate SDs ( $n = 3$ ). (i) Luciferase (LUC) complementation imaging (LCI) assays in *Nicotiana benthamiana* leaves showing the polymerization between the DRG1 (WT) and DRG1<sup>E209K</sup> (mutant) proteins. (j) Process of actin nucleation in the presence of DRG1 or DRG1<sup>E209K</sup> monitored by pyrene fluorescence every 60 s.

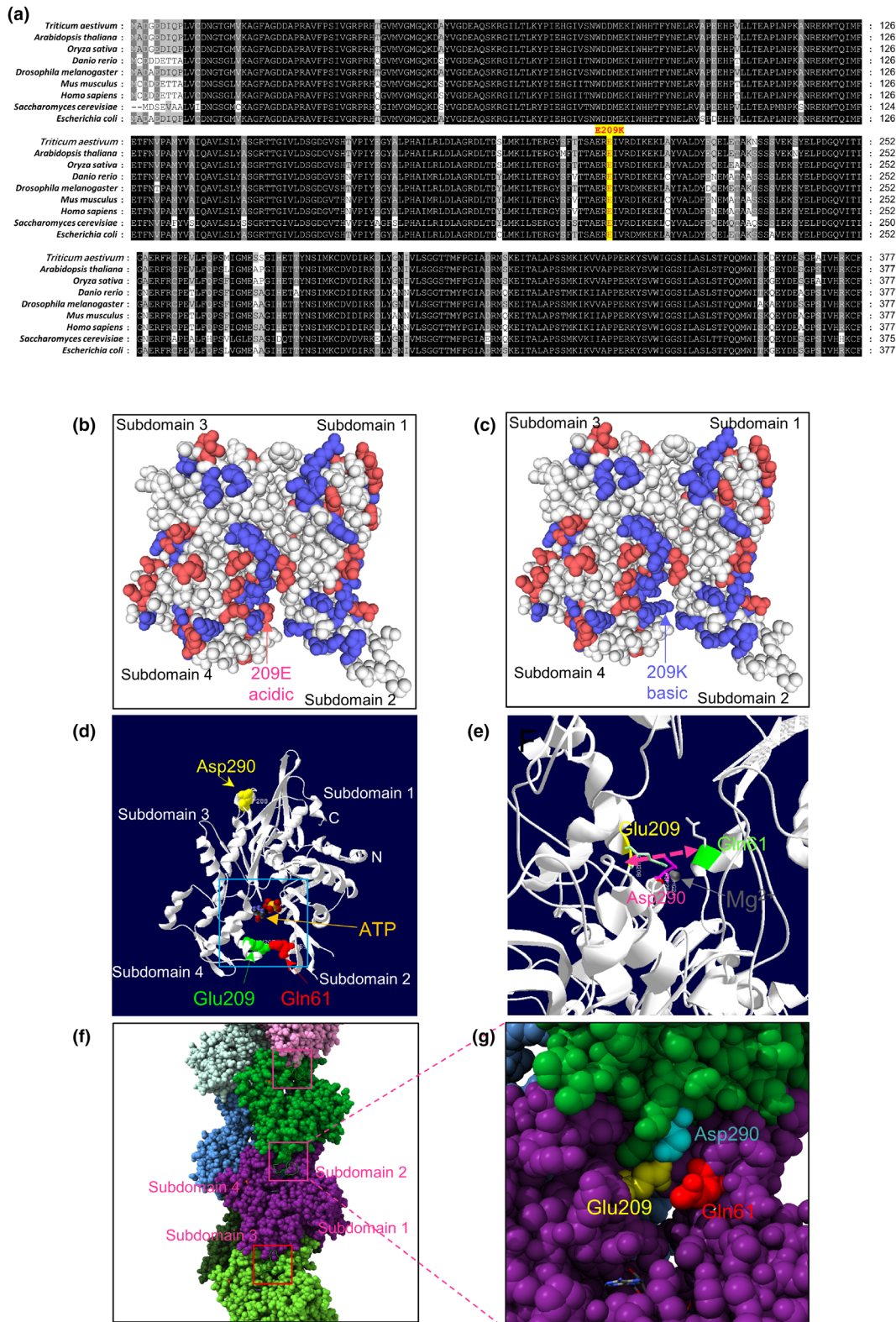


**Fig. 6** Protein sequence and structural analysis of DRG1. (a) Protein sequence alignment of DRG1 homologs from different species. The mutated amino acid is marked in red. (b, c) Structural modeling of the normal and mutated DRG1 monomer. Red, acidic amino acids. Blue, basic amino acids. Lysine is a basic amino acid with a positive net charge, and with a larger side chain than glutamic acid. (d) Structural modeling of the DRG1 monomer. Green, Glu209; red, Gln61; yellow, Asp290. The Glu209 and Gln61 amino acids of one monomer combine with the Asp290 of the other monomer to form a polymer. (e)  $Mg^{2+}$  forms an intramolecular bridge between Glu209 (yellow), Asp290 (pink), and Gln61 (green).  $Mg^{2+}$  is shown as a small gray ball. (f, g) Structural modeling of the DRG1 polymer. The polymerization locations of Asp290 (belonging to the upper monomer) and Gln61 and Glu209 (belonging to the lower monomer) are indicated in g. Yellow, Glu209; red, Gln61; blue, Asp290.

actins (Fig. 6b,g). The Glu209Lys substitution changes the properties of the amino acid and the structure of the amino acid side chain (Fig. 6b,c).  $Mg^{2+}$  with residues Glu209 and Asp290 reinforces the vertical interaction of MFs and also keeps the nucleotide-binding cleft closed through forming an intramolecular bridge with Gln61 and Glu209 (Fig. 6d,e). When Glu209Lys substitution occurs, the atoms in the side chain of Lys may occupy the space of the  $Mg^{2+}$  salt bridge, which would destroy the vertical interaction and sealing function to ATP (Fig. 6c–g). The Glu209Lys changes the charge of the amino acid and forms longer side chain, which would prevent the  $\gamma$ -phosphate from entering the Pi-release cavity (Fig. 6c–e). Consequently, the E209K may change the polymer extended direction and the stability of MFs.

### *drg1-D* affects the BR response

Studies have shown that BR can reorganize the actin cytoskeleton, altering the actin cytoskeleton in an auxin-like manner by unbundling actin filaments (Lanza *et al.*, 2012). Because of the abnormal response to BR in the *drg1-D* mutant, we examined the expression of some genes related to BR synthesis and signaling in both YZ1 and *drg1-D* mutant plants (Fig. 7a). Corresponding with the dwarf phenotype, expression of genes related to inhibition of cell elongation (*TaDLT*, *TaLIC*, *TaMDPI*, and *TaMADS2*) was upregulated in the *drg1-D* mutant (Fig. 7a). The expression levels of BR synthesis genes (*TaRAVL1*, *TaDWARF4*, *TaD11*, and *TaD2*) were also significantly increased in the *drg1-D* mutant (Fig. 7a). Consistent with this result, transcriptome analysis showed that the expression of six genes involved in BR synthesis pathways was upregulated in *drg1-D* mutant plants (Fig. S6; Tables S6–S10). BR biosynthesis is regulated by negative feedback. Normally, decreased BR content in plants can promote the expression of genes related to BR synthesis (Sun *et al.*, 2010; Zhao & Li, 2012). We therefore measured the content of BR (castasterone, 6-deoxoCS, and brassinolide) in YZ1 and *drg1-D* plants (Fig. S7). Surprisingly, the content of BR in mutant plants was significantly higher than in YZ1 plants (Fig. 7b). These results suggested that BR signal transduction was abnormal in *drg1-D* plants.

### Vesicular trafficking is disrupted in the *drg1-D* mutant

Because many important biological processes rely on functional MFs, we hypothesize that the cytoskeleton defect in the *drg1-D* mutant probably affects normal intracellular vesicular trafficking and BR signal transduction. Therefore, we examined the vesicular accumulation by staining the vesicles in the root cells of YZ1 and *drg1-D* mutant plants using FM4-64. Significantly, the fluorescence of vesicles in the *drg1-D* mutant was much stronger than that observed in YZ1 root cells (Fig. 7c–e). This result indicates that numerous vesicles could not be transported properly, leading to the accumulation of vesicles in the *drg1-D* mutant. This finding suggests that the amino acid substitution in DRG1 disrupts normal vesicular transport, which consequently altered the BR response and cell development.

## Discussion

In this study, we report the isolation and characterization of the dominant mutant *drg1-D* in wheat. The *DRG1* gene encodes an actin protein that plays a vital role in modulating cell size by regulating MF organization. Visualization of the MFs confirmed that the Glu209Lys substitution in the conserved domain of DRG1 is related to the disordered actin polymerization and MF organization in wheat. We hypothesized that the polymerization of DRG1<sup>E209K</sup> causes the MFs to polymerize in the wrong direction and reduces the number of MFs (Fig. 7f,g). Furthermore, DRG1<sup>E209K</sup> affects the expression of genes related to BR synthesis and signal transduction, leading to the BR-insensitive phenotypes. The *DRG1* gene regulates the actin cytoskeleton, BR signaling, and vesicular transport in wheat. Therefore, this gene and the particular mutation that results in the Glu209Lys substitution play a key role in cell shape determination, and this directly affects plant architecture and grain shape.

### Studying the *drg1-D* gene improves our understanding of actin structure and polymerization

The actin protein is highly conserved in all eukaryotes (Thyssen *et al.*, 2017). During the evolution of higher eukaryotes, the number of actin genes increased. In yeast, there is only one copy of the actin gene (Kovar *et al.*, 2011). In mammals, there are usually six different genes that encode actin subtypes. In plants, there are many more extra actin genes; for example, Arabidopsis has eight genes and hexaploid wheat has 17 actin genes (Table S5). Changes in particular amino acids during evolution have resulted in functional differentiation of some actin proteins (Gunning *et al.*, 2015; Velle & Fritz-Laylin, 2019). However, relatively few changes have occurred in actin during evolution. According to our study, the DRG1 sequence is 84.08% identical to yeast actin and 88.86% identical to human actin. The amino acid sequence similarities between DRG1 and AtACT2, AtACT7, and AtACT8 are 91.78%, 97.35%, and 92.04%, respectively. There are only 10 amino acid changes between DRG1 and AtACT7. The amino acid residue at position 209 in DRG1 is conserved in actin proteins in all species (Fig. 6a). This highly conserved site may be necessary for the formation of functional MFs. Our results suggested that specific amino acid substitutions in actin may alter actin polymerization. In humans, many actin mutations have been found to be pathogenic and cause a range of congenital disorders such as myopathy and deafness (Bryan *et al.*, 2006; Marston, 2018). Predicting the effects of each amino acid mutation is an effective approach to understanding their functions. The gain-of-function mutation in DRG1<sup>E209K</sup> is a valuable resource for the longer-term tools to better understand the polymerization of actin and its assembly into filaments and arrays.

### The study of the *drg1-D* mutant reveals the regulatory roles of actin in cell development in polyploid wheat

The model plants *Arabidopsis thaliana* and rice (*Oryza sativa*) are diploid. Mutations in conserved structural genes often have lethal

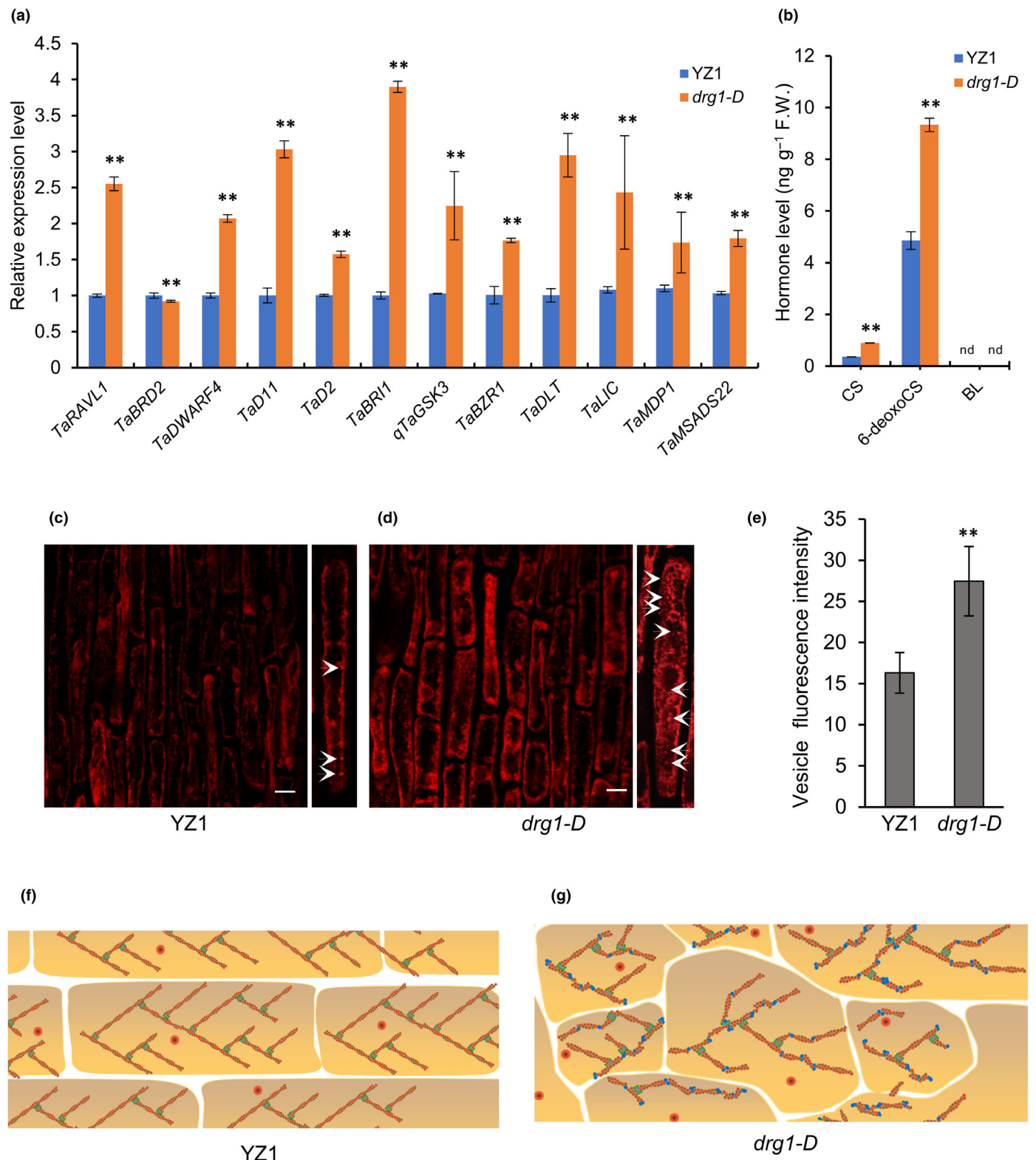


**Fig. 7** BR-related gene detection, vesicle observation, and MF pattern graph in YZ1 and *drg1-D* plants. (a) Expression analysis of genes from BR biosynthesis and signaling pathways in YZ1 and *drg1-D* plants. Values are means, \*\*,  $P < 0.01$ , significant differences (Student's *t*-test), with bars showing the SDs ( $n = 3$ ). (b) Comparison of the levels of castasterone (CS), 6-deoxoCS (two precursors involved in BR synthesis), and brassinolide (BL) between YZ1 and *drg1-D* plants. The levels of CS and 6-deoxoCS increased significantly in *drg1-D* plants. Values are means, \*\*,  $P < 0.01$ , significant differences (Student's *t*-test), with bars showing the SDs ( $n = 3$ ). nd, not detected. (c–e) Vesicle staining in YZ1 and the *drg1-D* mutant. The number of vesicles observed in the root cells of the *drg1-D* mutant increased significantly. The red dots pointed by the white arrows are vesicles. \*\*,  $P < 0.01$ , significant differences (Student's *t*-test). Error bars indicate SDs ( $n = 10$ ). Bars: 10  $\mu\text{m}$ . (f, g) The 'break subunit' model of DRG1 and the mutant DRG1 protein. The polymerization of DRG1<sup>E209K</sup> causes the polymerized microfilaments (MFs) to be unstable and leads to the wrong direction.

effects in these species, making it difficult to study the regulatory functions of these genes. In polyploids, multiple copies can compensate for the deleterious effects on the organism caused by a point mutation in an actin gene. The F-actin network can still be formed in *drg1-D* mutant cells, because Glu209Lys F-actin represents only a small fraction of the abundant actin protein (Table S5). In *drg1-D* heterozygous plants, the Glu209Lys mutation disrupts actin polymerization and the extension of the actin filaments, resulting in a defective actin cytoskeleton. As a result, *drg1-D* homozygous mutant plants exhibit a much more distorted phenotype compared with that observed in heterozygous plants. In polyploid wheat, there are extra copies in subgenomes, which could compensate the gene deletion in one subgenome. Therefore, a destructive mutation in wheat actin gene is easier to survive compared with diploid species carrying the same mutation. Thus, we can see how DRG1<sup>E209K</sup> affects cytoskeletal organization and cell shape determination.

### BR signaling is affected by the abnormal cytoskeleton in *drg1-D* mutant cells

It has been reported that BR can regulate the formation of the actin cytoskeleton by altering the bundling of actin filaments. The actin cytoskeleton functions as an integration node for the BR signaling pathway and the auxin response (Lanza *et al.*, 2012). Although the control of BR biosynthesis and the signal process has been demonstrated, the molecular basis of BR transport is not known. Other researchers have speculated that the transportation of BR requires functional vesicular transport (Vukašinović & Russinova, 2018). The feedback loop of BRI1 also relies on proper microtubule-dependent vesicular transport (Ruan *et al.*, 2018). The interrupted vesicular transport probably affected both BR transport and BRI localization (Fig. 7a). The BR content significantly increased in the *drg1-D* mutant (Figs 7b, S7a–i), and the expression of genes related to BR synthesis was increased in *drg1-D* mutant plants (Figs 7a, S6; Table S10), which is consistent with our hypothesis. We think that the reduction in the number of MFs resulted in abnormal vesicular transport, which led to the altered BR signaling and irregular cell development observed in the *drg1-D* mutant. Our study identified a wheat gene, which has potential applications in wheat breeding programs. The E209K mutation of DRG1/TaACT7 disrupts MF formation, which is useful for further studying the mechanisms controlling proper actin structures required for efficient cell and organ growth.

### Acknowledgements

This research was supported by the National Natural Science Foundation of China (31991213 and 91935304), Grant from Ministry of Agriculture and Rural Affairs of China, Talent Program and Agricultural Science and the Technology Innovation Program of CAAS. We thank Prof. Shanjin Huang (Center for Plant Biology, School of Life Sciences, Tsinghua University, Beijing, China) for providing experimental guidance. Thanks to Jiejie Li and Junxiu Hou for helping skewness analysis. Thanks to

Lingli Zheng for helping with wheat genetic transformation and Wuman Xu for helping manage the materials in the field.


### Competing interests

None declared.

### Author contributions

XK, CX and XL designed and supervised this study. ZX, LZ, QZ, YL, CD and DL performed research. XK, LZ, XL, ZX and CX analyzed the data. ZX, XK and CX wrote the paper. ZX and LZ contributed equally to this work.

### ORCID

Chunhao Dong  <https://orcid.org/0009-0004-6430-0683>  
 Xiuying Kong  <https://orcid.org/0000-0001-7447-395X>  
 Danping Li  <https://orcid.org/0000-0002-0201-409X>  
 Chuan Xia  <https://orcid.org/0009-0003-2991-3866>  
 Zhencheng Xie  <https://orcid.org/0009-0002-9693-7289>  
 Lichao Zhang  <https://orcid.org/0000-0001-9602-3079>  
 Qiang Zhang  <https://orcid.org/0000-0003-0325-6717>

### Data availability

The data of this study are available in the [Supporting Information](#).

### References

- Aya K, Hobo T, Sato-Izawa K, Ueguchi-Tanaka M, Kitano H, Matsuoka M. 2014. A novel AP2-type transcription factor, SMALL ORGAN SIZE1, controls organ size downstream of an auxin signaling pathway. *Plant and Cell Physiology* 55: 897–912.
- Bryan KE, Wen KK, Zhu M, Rendtorff ND, Feldkamp M, Tranebjærger L, Friderici KH, Rubenstein PA. 2006. Effects of human deafness gamma-Actin mutations (DFNA20/26) on Actin function. *The Journal of Biological Chemistry* 281: 20129–20139.
- Buschmann H, Fabri CO, Hauptmann M, Hutzler P, Laux T, Lloyd CW, Schäffner AR. 2004. Helical growth of the Arabidopsis mutant *tortifolia1* reveals a plant-specific microtubule-associated protein. *Current Biology* 14: 1515–1521.
- Cao Y, Huang H, Yu Y, Dai H, Hao H, Zhang H, Jiang Y, Ding M, Li F, Tu L *et al.* 2021. A modified Actin (Gly65Val substitution) expressed in cotton disrupts polymerization of Actin filaments leading to the phenotype of Ligon Lintless-1 (*Li1*) mutant. *International Journal of Molecular Sciences* 22: 3000.
- Chen H, Zou Y, Shang Y, Lin H, Wang Y, Cai R, Tang X, Zhou JM. 2008. Firefly luciferase complementation imaging assay for protein–protein interactions in plants. *Plant Physiology* 146: 323–324.
- Cheng X, Xin M, Xu R, Chen Z, Cai W, Chai L, Xu H, Jia L, Feng Z, Wang Z *et al.* 2020. A single amino acid substitution in STKc\_GSK3 kinase conferring semispherical grains and its implications for the origin of *Triticum sphaerococcum*. *Plant Cell* 32: 923–934.
- Cvrčková F, Oulehlová D, Žárský V. 2015. Formins, linking cytoskeleton and endomembranes in plant cells. *International Journal of Molecular Sciences* 16: 1–18.
- Engler C, Kandzia R, Marillonnet S. 2008. A one pot, one step, precision cloning method with high throughput capability. *PLoS ONE* 3: e3647.
- Feng G, Liu G, Xiao J. 2015. The Arabidopsis EIN2 restricts organ growth by retarding cell expansion. *Plant Signaling and Behavior* 10: e1017169.

- Gunning PW, Ghoshdastider U, Whitaker S, Popp D, Robinson RC. 2015. The evolution of compositionally and functionally distinct Actin filaments. *Journal of Cell Science* 128: 2009–2019.
- Hedden P. 2003. The genes of the green revolution. *Trends in Genetics* 19: 5–9.
- Higaki T, Kutsuna N, Sano T, Kondo N, Hasezawa S. 2010. Quantification and cluster analysis of Actin cytoskeletal structures in plant cells: role of Actin bundling in stomatal movement during diurnal cycles in Arabidopsis guard cells. *The Plant Journal* 61: 156–165.
- Hong Z, Ueguchi-Tanaka M, Umemura K, Uozu S, Fujioka S, Takatsuto S, Yoshida S, Ashikari M, Kitano H, Matsuoka M. 2003. A rice brassinosteroid-deficient mutant, *ebisu dwarf*(*d2*), is caused by a loss of function of a new member of cytochrome P450. *Plant Cell* 15: 2900–2910.
- Huang Y, Dong H, Mou C, Wang P, Hao Q, Zhang M, Wu H, Zhang F, Ma T, Miao R *et al.* 2022. Ribonuclease H-like gene *SMALL GRAIN2* regulates grain size in rice through brassinosteroid signaling pathway. *Journal of Integrative Plant Biology* 64: 1883–1900.
- Ishida Y, Tsunashima M, Hiei Y, Komari T. 2015. Wheat (*Triticum aestivum* L.) transformation using immature embryos. *Methods in Molecular Biology* 1223: 189–198.
- Isidro J, Knox R, Singh A, Clarke F, Krishna P, DePauw R, Clarke J, Somers D. 2012. Brassinosteroid leaf unrolling QTL mapping in durum wheat. *Planta* 236: 273–281.
- Jia J, Zhao S, Kong X, Li Y, Zhao G, He W, Appels R, Pfeifer M, Tao Y, Zhang X *et al.* 2013. *Aegilops tauschii* draft genome sequence reveals a gene repertoire for wheat adaptation. *Nature* 496: 91–95.
- Kato T, Morita MT, Tasaka M. 2010. Defects in dynamics and functions of Actin filament in Arabidopsis caused by the dominant-negative Actin *fiz1*-induced fragmentation of Actin filament. *Plant and Cell Physiology* 51: 333–338.
- Kovar DR, Sirotkin V, Lord M. 2011. Three's Company: the fission yeast Actin cytoskeleton. *Trends in Cell Biology* 21: 177–187.
- Lanza M, Garcia-Ponce B, Castrillo G, Catarecha P, Sauer M, Rodriguez-Serrano M, Páez-García A, Sánchez-Bermejo E, Leo del Puerto Y, Mohan TC *et al.* 2012. Role of Actin cytoskeleton in brassinosteroid signaling and in its integration with the auxin response in plants. *Developmental Cell* 22: 1275–1285.
- Li G, Liang W, Zhang X, Ren H, Hu J, Bennett MJ, Zhang D. 2014. Rice Actin-binding protein RMD is a key link in the auxin-Actin regulatory loop that controls cell growth. *Proceedings of the National Academy of Sciences, USA* 111: 10377–10382.
- Li J, Henty-Ridilla JL, Huang S, Wang X, Blanchoin L, Staiger CJ. 2012. Capping protein modulates the dynamic behavior of Actin filaments in response to phosphatidic acid in Arabidopsis. *Plant Cell* 24: 3742–3754.
- Li N, Xu R, Li Y. 2019. Molecular networks of seed size control in plants. *Annual Review of Plant Biology* 70: 435–463.
- Li S, Blanchoin L, Yang Z, Lord EM. 2003. The putative Arabidopsis Arp2/3 complex controls leaf cell morphogenesis. *Plant Physiology* 132: 2034–2044.
- Livak KJ, Schmittgen TD. 2001. Analysis of relative gene expression data using real-time quantitative PCR and the  $2^{-\Delta\Delta CT}$  Method. *Methods* 25: 402–408.
- Lu Y, Zhao T, Liu G, Jia J, Kong X. 2014. Identification and analysis of the dwarf-spherical grain mutant *w98*. *Journal of Plant Genetic Resources* 15: 160–164.
- Marston S. 2018. The molecular mechanisms of mutations in Actin and myosin that cause inherited myopathy. *International Journal of Molecular Sciences* 19: 2020.
- McDowell JM, Huang S, McKinney EC, An YQ, Meagher RB. 1996. Structure and evolution of the Actin gene family in *Arabidopsis thaliana*. *Genetics* 142: 587–602.
- Meagher RB, McKinney EC, Vitale AV. 1999. The evolution of new structures: clues from plant cytoskeletal genes. *Trends in Genetics* 15: 278–284.
- Michelot A, Guérin C, Huang S, Ingouff M, Richard S, Rodiuc N, Staiger CJ, Blanchoin L. 2005. The formin homology 1 domain modulates the Actin nucleation and bundling activity of Arabidopsis FORMIN1. *Plant Cell* 17: 2296–2313.
- Mori M, Nomura T, Ooka H, Ishizaka M, Yokota T, Sugimoto K, Okabe K, Kajiwara H, Satoh K, Yamamoto K *et al.* 2002. Isolation and characterization of a rice dwarf mutant with a defect in brassinosteroid biosynthesis. *Plant Physiology* 130: 1152–1161.
- Nakagawa H, Tanaka A, Tanabata T, Ohtake M, Fujioka S, Nakamura H, Ichikawa H, Mori M. 2012. *SHORT GRAIN1* decreases organ elongation and brassinosteroid response in rice. *Plant Physiology* 158: 1208–1219.
- Nishimura T, Yokota E, Wada T, Shimmen T, Okada K. 2003. An Arabidopsis *ACT2* dominant-negative mutation, which disturbs F-Actin polymerization, reveals its distinctive function in root development. *Plant and Cell Physiology* 44: 1131–1140.
- Peng D, Chen X, Yin Y, Lu K, Yang W, Tang Y, Wang Z. 2014. Lodging resistance of winter wheat (*Triticum aestivum* L.): Lignin accumulation and its related enzymes activities due to the application of paclobutrazol or gibberellin acid. *Field Crops Research* 157: 1–7.
- Pollard TD, Cooper JA. 2009. Actin, a central player in cell shape and movement. *Science* 326: 1208–1212.
- Ruan Y, Halat LS, Khan D, Jancowski S, Ambrose C, Belmonte MF, Wasteneys GO. 2018. The microtubule-associated protein CLASP sustains cell proliferation through a brassinosteroid signaling negative feedback loop. *Current Biology* 28: 2718–2729.
- Song L, Liu J, Cao B, Liu B, Zhang X, Chen Z, Dong C, Liu X, Zhang Z, Wang W *et al.* 2023. Reducing brassinosteroid signalling enhances grain yield in semi-dwarf wheat. *Nature* 617: 118–124.
- Sun T, Li S, Ren H. 2017. OsFH15, a class I formin, interacts with microfilaments and microtubules to regulate grain size via affecting cell expansion in rice. *Scientific Reports* 7: 6538.
- Sun Y, Fan XY, Cao DM, Tang W, He K, Zhu JY, He JX, Bai MY, Zhu S, Oh E *et al.* 2010. Integration of brassinosteroid signal transduction with the transcription network for plant growth regulation in Arabidopsis. *Developmental Cell* 19: 765–777.
- Sun Y, Liang W, Shen W, Feng H, Chen J, Si Z, Hu Y, Zhang T. 2019. G65V substitution in Actin disturbs polymerization leading to inhibited cell elongation in cotton. *Frontiers in Plant Science* 10: 1468.
- Tanabe S, Ashikari M, Fujioka S, Takatsuto S, Yoshida S, Yano M, Yoshimura A, Kitano H, Matsuoka M, Fujisawa Y *et al.* 2005. A novel cytochrome P450 is implicated in brassinosteroid biosynthesis via the characterization of a rice dwarf mutant, *dwarf11*, with reduced seed length. *Plant Cell* 17: 776–790.
- Thyssen GN, Fang DD, Turley RB, Florane CB, Li P, Mattison CP, Naoumkin M. 2017. A Gly65Val substitution in an Actin, GhACT\_LL11, disrupts cell polarity and F-Actin organization resulting in dwarf, lintless cotton plants. *The Plant Journal* 90: 111–121.
- Tong H, Liu L, Jin Y, Du L, Yin Y, Qian Q, Zhu L, Chu C. 2012. DWARF AND LOW-TILLERING acts as a direct downstream target of a GSK3/*SHAGGY*-like kinase to mediate brassinosteroid responses in rice. *Plant Cell* 24: 2562–2577.
- Velle KB, Fritz-Laylin LK. 2019. Diversity and evolution of Actin-dependent phenotypes. *Current Opinion in Genetics and Development* 58–59: 40–48.
- Vukašinović N, Russinova E. 2018. BRexit: possible brassinosteroid export and transport routes. *Trends in Plant Science* 23: 285–292.
- Wang B, Smith SM, Li J. 2018. Genetic regulation of shoot architecture. *Annual Review of Plant Biology* 69: 437–468.
- Wang N, Xing Y, Lou Q, Feng P, Liu S, Zhu M, Yin W, Fang S, Lin Y, Zhang T *et al.* 2017. *Dwarf and short grain 1*, encoding a putative U-box protein regulates cell division and elongation in rice. *Journal of Plant Physiology* 209: 84–94.
- Wu S, Xie Y, Zhang J, Ren Y, Zhang X, Wang J, Guo X, Wu F, Sheng P, Wang J *et al.* 2015. *VLN2* regulates plant architecture by affecting microfilament dynamics and polar auxin transport in rice. *Plant Cell* 27: 2829–2845.
- Xing HL, Dong L, Wang ZP, Zhang HY, Han CY, Liu B, Wang XC, Chen QJ. 2014. A CRISPR/Cas9 toolkit for multiplex genome editing in plants. *BMC Plant Biology* 14: 327.
- Yang W, Ren S, Zhang X, Gao M, Ye S, Qi Y, Zheng Y, Wang J, Zeng L, Li Q *et al.* 2011. *Bent UPPERMOST INTERNODE1* encodes the class II formin FH5 crucial for Actin organization and rice development. *Plant Cell* 23: 661–680.
- Yang Y, Zhang X, Wu L, Zhang L, Liu G, Xia C, Liu X, Kong X. 2021. Transcriptome profiling of developing leaf and shoot apices to reveal the molecular mechanism and co-expression genes responsible for the wheat heading date. *BMC Genomics* 22: 468.



- Zhang L, Wang R, Xing Y, Xu Y, Xiong D, Wang Y, Yao S. 2021. Separable regulation of POW1 in grain size and leaf angle development in rice. *Plant Biotechnology Journal* 19: 2517–2531.
- Zhao B, Li J. 2012. Regulation of brassinosteroid biosynthesis and inactivation. *Journal of Integrative Plant Biology* 54: 746–759.
- Zhu J, Bailly A, Zwiewka M, Sovero V, Di Donato M, Ge P, Oehri J, Aryal B, Hao P, Linnert M *et al.* 2016. Twisted DWARF1 mediates the action of auxin transport inhibitors on Actin cytoskeleton dynamics. *Plant Cell* 28: 930–948.

## Supporting Information

Additional Supporting Information may be found online in the Supporting Information section at the end of the article.

**Fig. S1** Phenotypes of *drg1-D* mutant and YZ1 plants.

**Fig. S2** BR treatment and stem observation in the YZ1 and *drg1-D* plants.

**Fig. S3** Leaf and stem phenotypes in the *gdrg1-D* transgenic wheat lines.

**Fig. S4** Sequence analysis of DRG1 family proteins.

**Fig. S5** Leaf and stem phenotypes in the *DRG1-edited* transgenic lines.

**Fig. S6** KEGG term enrichment and Mapman analysis of DEGs in *drg1-D* backcross mutants.

**Fig. S7** UHPLC–MS/MS chromatograms of BRs in YZ1 and *drg1-D*.

**Table S1** Primers and sequences used in this study.

**Table S2** Phenotypic performance of YZ1 and *drg1-D* mutant.

**Table S3** Detailed information of nine annotated genes in the 275-kb region.

**Table S4** Sequences of gene editing mutant lines by CRISPR/Cas9.

**Table S5** Homologous genes and expression levels of *DRG1*.

**Table S6** KEGG term enrichment analysis of DEGs in *drg1-D* backcross mutants.

**Table S7** GO term enrichment analysis of DEGs in *drg1-D* backcross mutants.

**Table S8** Annotation of upregulated differentially expressed genes (DEGs) in *drg1-D* backcross mutants.

**Table S9** Annotation of downregulated differentially expressed genes (DEGs) in *drg1-D* backcross mutants.

**Table S10** DEGs associated with BR synthesis were functionally annotated by Mapman.

Please note: Wiley is not responsible for the content or functionality of any Supporting Information supplied by the authors. Any queries (other than missing material) should be directed to the *New Phytologist* Central Office.